Front. Struct. Civ. Eng. 2014, 8(3): 292–307
DOI 10.1007/s11709-014-0256-8

CASE STUDY

Liquefaction assessment using microtremor measurement, conventional method and artificial neural network (Case study: Babol, Iran)

Sadegh REZAEI*, Asskar Janalizadeh CHOOBBASTI

Department of Civil Engineering, Babol University of Technology, Babol P.O. Box 484, Iran
**Corresponding author. E-mail: S_Rezaei1366@yahoo.com*

ABSTRACT Recent researchers have discovered microtremor applications for evaluating the liquefaction potential. Microtremor measurement is a fast, applicable and cost-effective method with extensive applications. In the present research the liquefaction potential has been reviewed by utilization of microtremor measurement results in Babol city. For this purpose microtremor measurements were performed at 60 measurement stations and the data were analyzed by suing Nakmaura's method. By using the fundamental frequency and amplification factor, the value of vulnerability index (K_g) was calculated and the liquefaction potential has been evaluated. To control the accuracy of this method, its output has been compared with the results of Seed and Idriss [1] method in 30 excavated boreholes within the study area. Also, the results obtained by the artificial neural network (ANN) were compared with microtremor measurement. Regarding the results of these three methods, it was concluded that the threshold value of liquefaction potential is $K_g = 5$. On the basis of the analysis performed in this research it is concluded that microtremors have the capability of assessing the liquefaction potential with desirable accuracy.

KEYWORDS liquefaction, microtremor, vulnerability index, artificial neural networks (ANN), microzonation

1 Introduction

Earthquake is one of the most devastating natural disasters which has always threatens human lives and properties. The most important effects caused by an earthquake are the liquefaction phenomena. Investigations of failures of soil masses are subjects touching both geology and engineering [2].

The release of potential energy in the earth crust due to slip along an existing fault may produce rapid accelerations and consequently additional internal stresses. The produced rapid acceleration and the additional internal stresses may cause the already existing in situ shear stress along a potential failure plane to increase. Furthermore, due to the shaking the material may tend to densify, which may lead to an excess pore pressure in saturated loose soil and consequently to a reduction of the normal effective stresses. Liquefaction of soils is a consequence of the buildup of large excess pore pressure due to partially undrained deformation of loose soils, leading to a relatively small undrained shear strength compared to the shear strength for drained behavior [3].

On the basis of both the field and the laboratory types of observations of soil behavior attempts were made to propose methods to evaluate the liquefaction potential of a particular soil.

Recently, the H/V technique [4] is becoming more popular with its data collection facilities and application allowance in all areas [5–9]. By employing the H/V ratio, we were able to determine the predominant frequency (F_P) and the amplification factor (A_P) of the site. Nakamura [10] also proposed the vulnerability index "K_g value" as a means to determine the extent of liquefaction. The present study mainly aims to show how the microtremor measurements can play a significant role in a liquefaction assessment [11].

Article history: Received Jan. 14, 2014; Accepted Apr. 24, 2014

Microtremor measurement was undertaken at 60 stations in the Babol, north of Iran, during 2011 and 2012. The study was conducted in Babol city for one important reason: the city is densely populated with critical buildings and infrastructures and it is built upon the recent, loose, and therefore, generally liquefaction-prone sediments of the Babolrood River. With regards Nakamura's method, H/V spectral ratios, fundamental frequency and amplification factor and finally vulnerability index (K_g) were calculated for all microtremor stations.

There are geotechnical boreholes near 30 microtremor recording stations with suitable data. The Seed and Idriss [1] method is used to assess the liquefaction potential. This method proposes using the estimated shear stress level and cycle number likely to be developed in the field, due to a design earthquake. Comparison of these stresses with those causing liquefaction of soil helps in identifying the liquefiable zones of a deposit.

Furthermore, the artificial neural network (ANN) with different inputs including soil type, total stress, effective stress, corrected SPT blow count was trained. Then the trained ANN predicts the liquefaction potential and the output results were compared with microtremor results. The goal of the aim activities includes the assessment of liquefaction by a new, fast and applicable method in other stations and preparation of Babol city's liquefaction map. Successful prediction of liquefaction in soil deposit using the existing data leads to improve the reliability of data which will be used for construction in future [12,13].

2 Seismology and geology of Babol

Unfortunately, Iran's human communities and material infrastructure have been developed in disaster prone areas such as the Babol city. Population in these communities have been increased, therefore an accurate natural hazard risk assessment is necessary. Accordingly, study of the risk of earthquake and estimation of ground motion parameter and also liquefaction assessment of ground against earthquake damage caused by the earthquake in point of view science of seismology and earthquake engineering and economic development projects are of great importance. So it is up to the importance and risk of each project to be conducted by design or retrofitted in contrast to earthquake based on the design parameters and appropriate methods until secure performance is provided.

Babol is located in front of Alborz mountain range which is tectonically an active region situated between the Caspian Sea and the Iran platform. The tectonic of Alborz Mountain is controlled by the boundary condition due to convergent motion between Arabia and Eurasia, which probably started in the Cretaceous. The area around Babol has repeatedly experienced earthquakes. Figure 1 shows the Location and magnitude of earthquakes, faults and their mechanism near the Babol. Also, Table 1 shows the length, mechanism and distance to study area of available faults over a radius of 200 km around Babol city.

Depending on the lithological variations through 30 boring logs in the city of Babol, the subsurface soil column at Babol city can be classified and is composed of the 5 following profileds:

1) Extremely loose to loose fine to medium sand deposits from the surface to 15 m depth with a very shallow groundwater table (less than 1 m).

2) Thin top layer of clay (3–5 m with SPT-N values from 15 to 20) underlain by thick layer of very loose to loose fine sand with some gravel (8–12 m with SPT-N values between 15 and 10) below the ground level.

3) Thick top layer of clay (8–15 m with SPT-N values

Table 1 The properties of available faults around the study area

fault name	distance to study area (km)	fault length (km)	fault mechanism
Firooz Abad	85	112	thrust fault
Alborz	44	300	thrust fault
Khazar	16	550	thrust fault
Attari	91	85	thrust fault
Astane	93	75	thrust fault
Garmsar	136	70	thrust fault
Kandovan	100	64	thrust fault
Masha	91	400	thrust fault
North of Tehran	115	108	thrust fault
Ivanaki	143	75	thrust fault
Firoozkooh	84	40	thrust fault
Basham	96	71	thrust fault
Ourim	72	44	thrust fault
Damghan	136	100	thrust fault

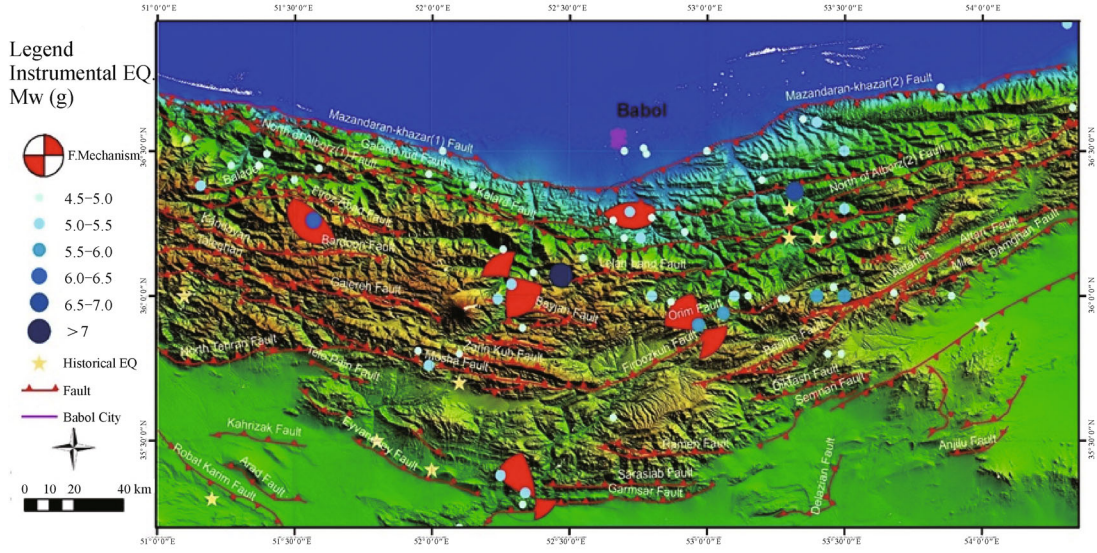

Fig. 1 Location and magnitude of earthquakes, Faults and their mechanism near the Babol

from 10 to 15) underlain by thin layer of loose fine sand with some gravel (3–6 m with SPT-N values between 15 and 20) below the ground level.

4) Thick layer of clay (20–30 m with SPT-N values from 20 to 25).

5) Thick layer of sand (15–20 m with SPT-N values from 15 to 25).

The city is located on the east bank of the river Babolrood and receives abundant annual rainfall [12]. The average depth of ground water in this region is 2.4 m. Based on the water level data in the geotechnical boreholes and also the seismic data inside the boreholes, the map for ground water level was prepared for babol city. Figure 2 shows the ground water distribution in Babol city.

Finally we can say this region consists of soft deposits and also located in a high seismic region. This fact shows it necessitates the assessment of liquefaction potential.

3 Methodology

Ambient seismic noise or microtremors are feeble ground motions with displacement amplitudes of about 0.1–1 μm and that can be detected by seismograph with high magnification [13–15]. Many investigations have been conducted to determine the nature of microtremors. One of the possible sources of microtremors can be human activity, such as traffic, industrial noises and nature activity, such as wind, ocean waves [15].

Previous studies related to the analysis of microtremor data and other example use of H/V ratios includes the evaluation of site effect [4,5,16], estimation of the depth of the seismic bedrock and engineering bedrock (e.g., [17]), evaluation of transfer functions (e.g., [18]), investigation of the response characteristics and assessment of the vulnerability of surface ground and structures (e.g., [19]) and seismic microzonation (e.g., [20]). Recently, to assess potential hazards associated with ground failure or liquefaction, the vulnerability index (or K_g value) that is derived from microtremor data may be evaluated. Among the various approaches to microtremor study, the H/V spectral ratio technique introduced by Nakamura [4] was chosen for this investigation due to ease of application. This technique has been described in a number of papers (e.g., [21–26]).

Site effects due to surface geology are generally expressed as the spectral ratio (S_T) between the horizontal tremor spectrum on the surface of the soft layer (S_{HS}) and the horizontal tremor spectrum incident from the substrate to surface layer (S_{HB}) (Fig. 3):

$$S_T = S_{HS}/S_{HB}. \quad (1)$$

But S_{HS} is readily affected by the surface wave. Since the artificial noise is mostly propagated as Rayleigh wave, S_{HS} of microtremor may possibly be affected by Rayleigh wave. The effect of Rayleigh wave should be included in the vertical tremor spectrum S_{VS} on the surface, but not included in the vertical tremor spectrum S_{VB} in the base ground (Fig. 3). Assuming that the vertical tremor is not amplified by the surface layers, the amount E_S defined below should represent the effect of Rayleigh wave on the vertical tremor:

$$E_S = E_{VS}/E_{VB}. \quad (2)$$

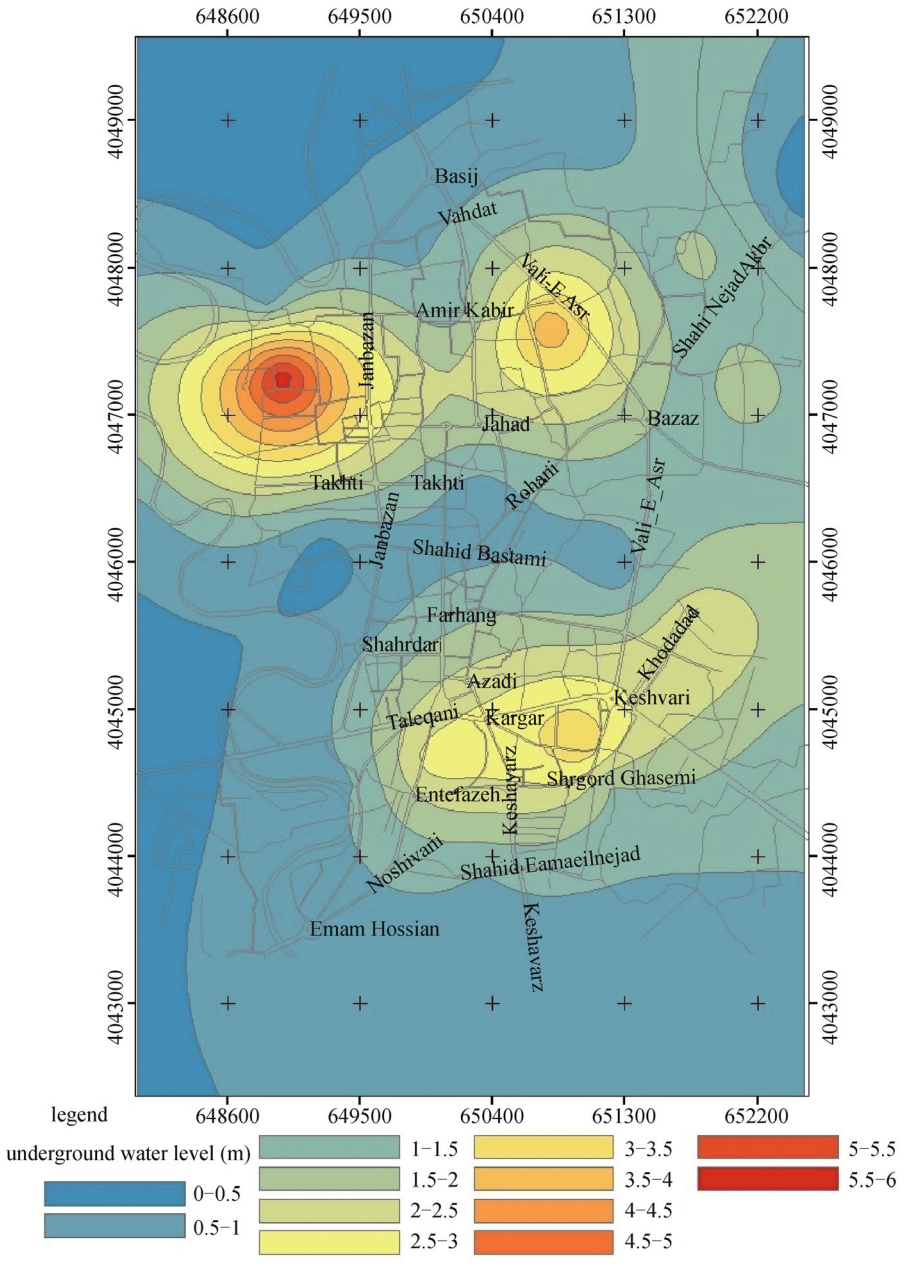

Fig. 2 map of ground water distribution in Babol city

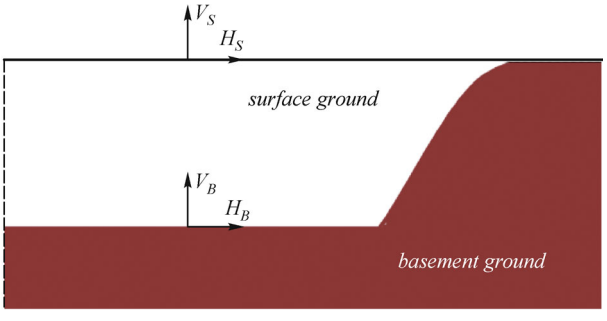

Fig. 3 Simple model assumed by Nakamura

If there is no Rayleigh wave, $E_S = 1$. E_S will take a value larger than "1" with increasing effect of Rayleigh wave.

Assuming that the effect of Rayleigh wave is equal for vertical and horizontal components, S_T/E_S may be considered to offer a more reliable transfer function S_{TT} after elimination of the effect of Rayleigh wave. Namely:

$$S_{TT} = S_T/E_S = R_S/R_B, \tag{3}$$

where $R_S = S_{HS}/S_{VS}$ and $R_B = S_{HB}/S_{VB}$. R_S and R_B were obtained by dividing the horizontal tremor spectrum by vertical spectrum, corresponding respectively to surface and substrate earthquake tremors. R_B becomes nearly 1 for

relatively wide frequency range. Namely, on the firm substrate, propagation is even in all directions. Namely,

$$R_B = 1. \tag{4}$$

Therefore,

$$S_{TT} = R_S. \tag{5}$$

This means that the transfer function of surface layers may be estimated from the tremor on the surface only. In other words, the vertical tremor on the surface retains the characteristics of horizontal tremor of the substrate [4,20,21,27].

By employing the H/V ratio, we were able to determine the predominant frequency (F_P) and the amplification factor (A_P) of the site. Nakamura [10] also proposed the vulnerability index "K_g value" as a means to determine the extent of liquefaction. For this purpose, he compared the results of vulnerability index and the damage points in the Kobe earthquake and concluded that K_g is a suitable index for determining the site vulnerable points, such that each point with higher K_g value is more damage potential. The K_g value is simply derived from strain of ground structures [10,19,28]. It can be defined as:

$$K_g = \frac{A_P}{F_P}. \tag{6}$$

After Nakamura some scientist have used microtremor to liquefaction evaluation [8,11,29,30].

In this study, the authors determined the site characteristics of the Babol city using the H/V of microtremors and the K_g values to predict the potential for soil liquefaction at the site.

4 Data collection, analysis procedures and measurement results

Microtemor measurements were carried out at 60 stations in Babol during the period 2011 and 2012. Figure 4 shows the location of microtremor recording stations and geotechnical boreholes available in the study area. The microtremor recording stations are shown with red circle and the geotechnical boreholes with blue circle.

Microtremor measurements were recorded using a velocity meter SARA. The SARA velocity sensors had a natural period of 2 s. There sensors were deployed for every measurement, two in two orthogonal horizontal directions and one in vertical directions. The amplifier unit improved the quality of the signals by extending the natural period to 5 s, filtering undesired frequencies and amplifying the signal. This data acquisition system comprises fully integrated triaxial high-sensitive sensors and includes a 24-bit A/D converter. Two horizontal and a vertical components of microtremors at each location are recorded for duration of 15 min with 100 samples per second. Because the environment has an effect on microtremors they are measured between 10 p.m. and 3 a.m. to reduce environmental noises during experimental. The locations were determined by using GPS at the sites. The microtremor measurements in this study were made in compliance with the guidelines of SESAME. In the framework of the European research project SESAME (Site Effects Assessment Using Ambient Excitations), the use of ambient vibrations in understanding local site effects has been studied in detail. The recommended guidelines on the H/V spectral ratio technique are the result of comprehensive and detailed analyses performed by the SESAME participants during the three years (2001–2004). In this respect, the guidelines represent the state-of-the-art of the present knowledge of this method and its applications, and are based on the consensus reached by a large group of participants. (SESAME Project, 2004 http://sesame-fp5.obs.ujf-grenoble.fr).

Processing starts from transforming data from the Binary format to ASCII. The processing was carried out by Geopsy software. For each station, the time-series of the record is divided into windows of 25 s duration. Each window is base-line corrected for anomalous trends, tapered with Hanning window and bandpass filtered from 0.2 to 20 Hz. The Fourier amplitude spectra of each selected window are computed and smoothed after which the two horizontal components are merged applying the geometric mean [31]. The H/V spectral ratio of Nakamura [4] is applied for each individual window and the final predominant frequency is obtained by averaging the H/V spectral ration as follows:

$$H_{avg}/V = \sqrt{\left(N^2(f) + E^2(f)/2\right)}/V(f), \tag{7}$$

where, N, E and V are the Fourier spectrum in NS, EW and UD direction respectively.

After obtaining the H/V spectra for appropriate windows, reliability and clarity of the peak in the H/V curve have been checked. For this purpose, we use the SESAME guidelines. For more information about SESAME research project and the criteria for a clear H/V peak and reliable H/V curve, visit (SESAME, 2004, http://sesame-fp5.obs.ujf-grenoble.fr).

Figure 5 shows the H/V spectral ratio for some stations. According to the analysis, the fundamental frequency (F_P) varies from 0.69 to 12.60 Hz within the study area. Also, the amplification factor (A_P) varies from 1.45 to 4 within the study area. Figures 6 and 7 show the fundamental frequency and amplification factor in the study area, respectively. As it can be observed in the Fig. 6 and Fig. 7 for 10 recording stations, fundamental frequency and amplification factor have not presented. Since these stations have been surrounded by the factories and highways in the city, accurate microtremor recording was impossible all day long.

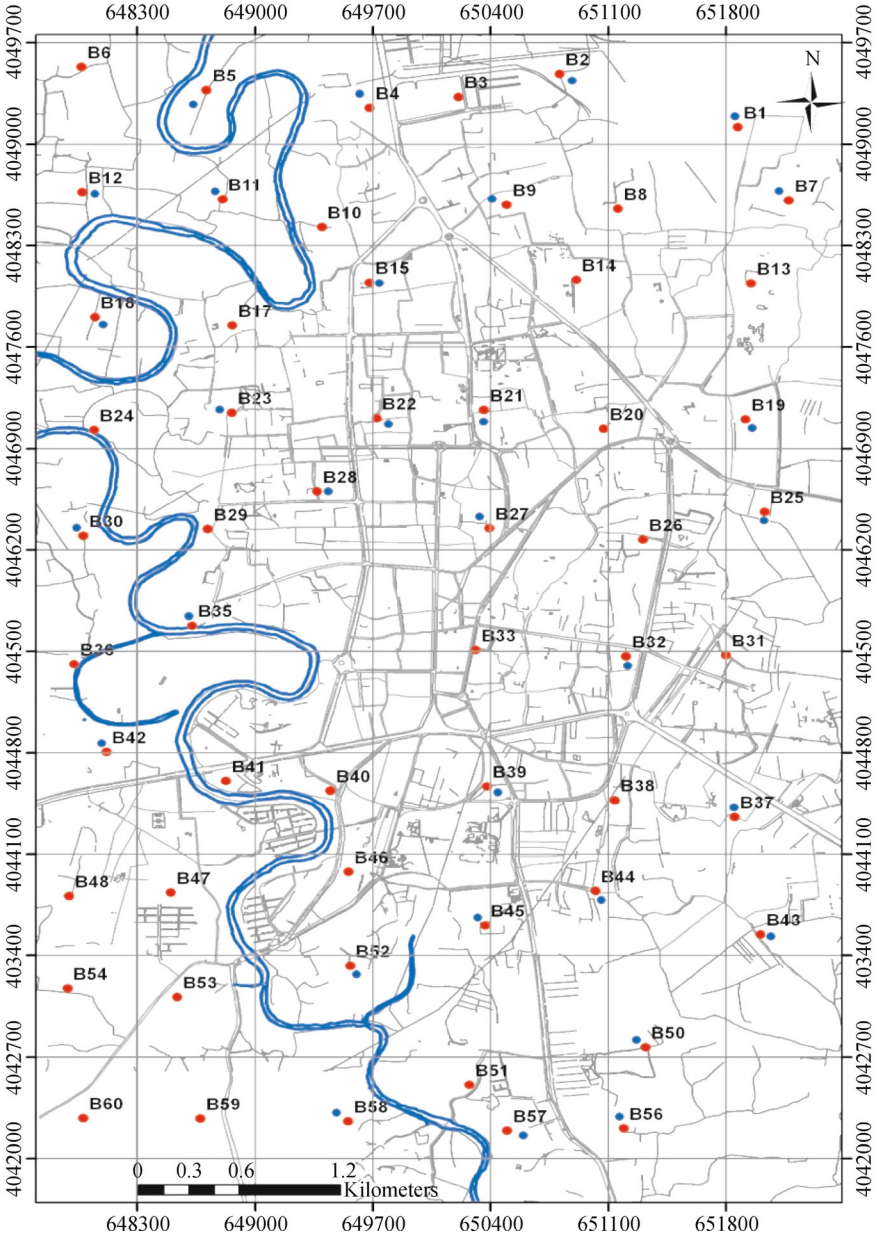

Fig. 4 Location of microtremor recording stations and geotechnical boreholes

By using the results of Figs. 6 and 7, the K_g values are calculated for different stations. These results are indicated in Fig. 8. By reviewing the scientific literature, it has been concluded that the higher K_g value, the more liquefaction potential will be. In fact K_g value has a qualitative meaning, for instance the possibility of liquefaction occurrence is more in recording station 35 than recording station 25.

Now to obtain a precise value for K_g which is the threshold value for liquefaction occurrence, one of the two methods below should be selected:

1) Reviewing the liquefaction areas after occurrence of earthquakes and comparing them with the K_g values obtained from microtremor measurement.

2) Evaluation the liquefaction potential by using conventional methods and comparing the related results with K_g values obtained from microtremor measurement.

In this research, the second method is used. In the next sections, first, the possibility of liquefaction occurrence will be evaluated by using the data of 30 geotechnical boreholes and the Seed and Idriss [1] method. Secondly, the ANN with different inputs including type of soil, total stress, effective stress and corrected SPT blow count was trained. Subsequently, by comparing the stations in which liquefaction has occurred (using Seed and Idriss [1] and ANN) and the values obtained from microtermor measurement, it was possible to obtain a precise value for K_g which is the threshold value for liquefaction occurrence.

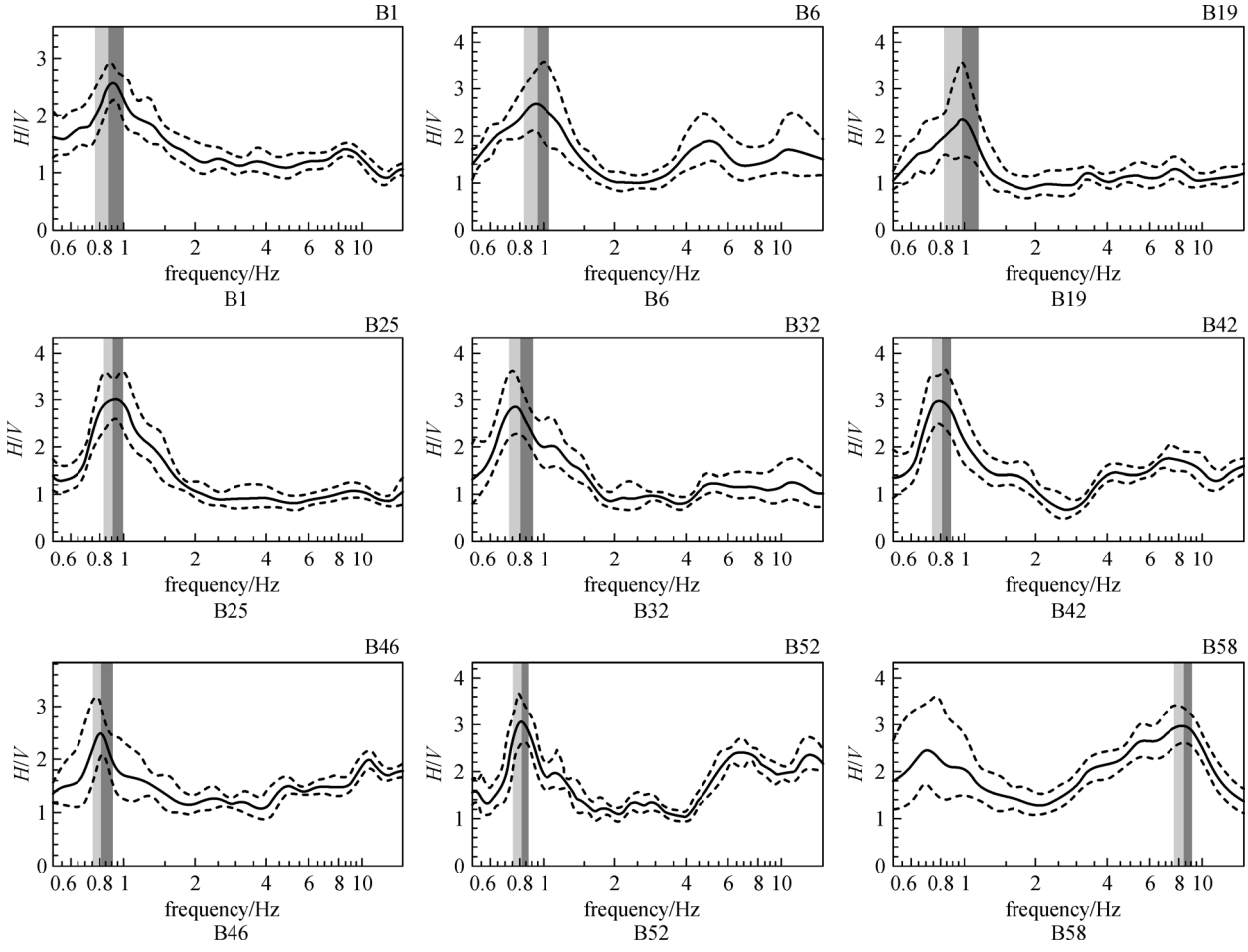

Fig. 5 *H*/*V* spectral ratio

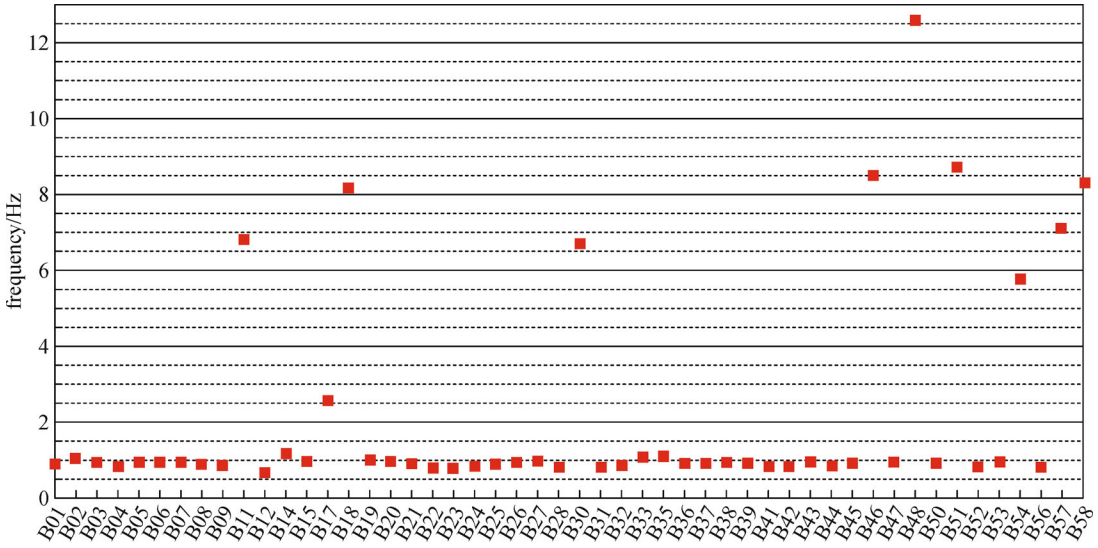

Fig. 6 Fundamental frequency

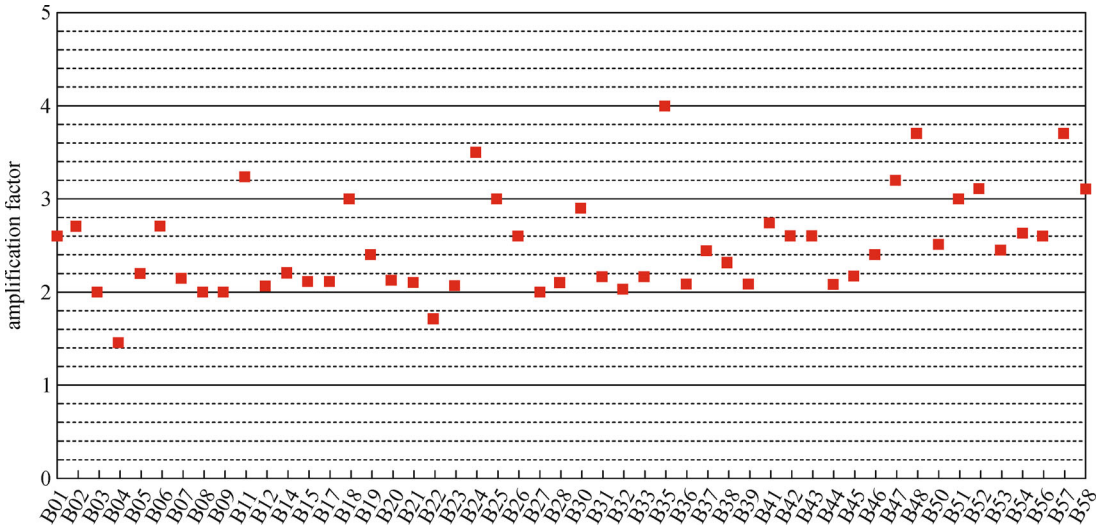

Fig. 7 Amplification factor

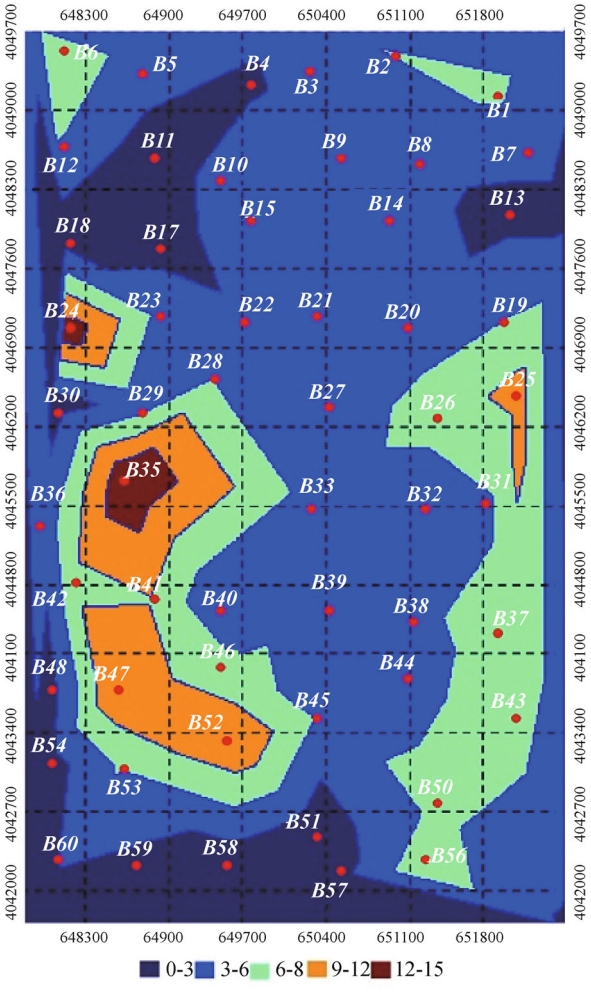

Fig. 8 map of K_g distribution in Babol city

5 Assessment and comparison of liquefaction potential by using conventional method

Simplified procedures, originally proposed by Seed and Idriss [1], using the standard penetration test (*SPT*), are frequently used to evaluate the liquefaction potential of soils. This procedure has been revised and updated since its original development [32]. The method was developed from field liquefaction performance cases at sites that had been characterized with in situ standard penetration tests. Using a deterministic method, liquefaction of soil is predicted to occur if the factor of safety (*FS*) which is the ratio of the cyclic resistance ratio (*CRR*) over cyclic stress ratio (*CSR*), is less than or equal to one. No soil liquefaction is predicted if $FS > 1$ [33].

For liquefaction evaluation, the cyclic stress ratio (*CSR*) has been proposed by Seed et al. [32] as

$$CSR = 0.65\frac{\sigma_v}{\sigma_v'}\frac{a_{max}}{g}\gamma_d, \tag{8}$$

where σ_v is the total vertical stress; σ_v' is the effective vertical stress; a_{max} is the peak horizontal ground surface acceleration; g is the acceleration of gravity; and γ_d is the stress reduction factor. Cyclic resistance ratio (*CRR*), the capacity of soil to resist liquefaction, can be obtained from the corrected blow count $(N_1)_{60}$ using empirical correlations proposed by Seed et al. [32]. *CRR* curves have been proposed for granular soils with fines contents of 5% or less, 15%, and 35% and are only valid for magnitude 7.5 earthquakes. The *CRR* curves for a fines content of $< 5\%$ (clean sands) can be approximated by [34]

$$CRR_{7.5} = \frac{1}{34-(N_1)_{60}} + \frac{(N_1)_{60}}{135} + \frac{50}{[10.(N_1)_{60}+45]^2} - \frac{1}{200}, \quad (9)$$

for $(N_1)_{60} < 30$. For $(N_1)_{60} > 30$, clean granular soils are classified as non-liquefiable. The *CRR* increases with increasing fines content and thus $(N_1)_{60}$ should be corrected to an equivalent clean sand value, $(N_1)_{60CS}$ [34]. The *FS* against liquefaction in terms of *CSR* and *CRR* is defined by

$$FS = \frac{CRR_{7.5}}{CSRN} K_\sigma K_\alpha, \quad (10)$$

where *CSRN* is the normalized *CSR* for earthquakes of magnitude 7.5 (CSR/MSF); *MSF* is the magnitude scaling factor; K_σ is the correction factor for effective overburden; and K_α is the correction factor for sloping ground. The consideration of factors K_σ and K_α is beyond routine practice and can be precisely estimated using the method of Youd et al. [34] if necessary. The term *MSF* is used to adjust the calculated *CSR* or *CRR* to the reference earthquake magnitude of 7.5.

An assessment of liquefaction potential can readily be made by Eq. (10). Liquefaction is predicted to occur if $FS \leqslant 1$, and no liquefaction is predicted if $FS > 1$ [33].

By using the 30 geotechnical boreholes in the region, we can assess the liquefaction potential in Babol city. The results of this assessment in 4 boreholes have been shown in Fig. 9. In these 30 boreholes we compare the two methods of conventional and microtremor and by analyzing the results it is possible to obtain a precise value for K_g which is the threshold value for liquefaction occurrence. Table 2 shows the depths of evaluated liquefaction using conventional method against the K_g value.

By reviewing Table 2, it is observed that in all the stations with K_g values higher than 5, liquefaction phenomena occurred. Consequently the value of $K_g = 5$ can be considered as a threshold value for these 30 stations, in that for all the stations of this region with K_g value higher than 5, the occurrence of liquefaction phenomena is possible and for stations with lesser values, this possibility does not exist.

In the next section, we assess the potential of liquefaction using ANN method and the results will be compared with the results of microtremor measurement to be able to prepare the liquefaction microzonation map of Babol city.

6 Artificial neural networks

Today, the application of artificial neural networks in the engineering world is well known to engineering sciences [35–37]. Goh [38] developed a back propagation neural network (BPNN) model to assess soil liquefaction. In his second neural network model for soil liquefaction potential evaluation, Goh [39] introduced a new field parameter, which is the cone penetration resistance, to the model and removed SPT-N value parameter. In his further study, Goh

Table 2 The liquefaction depths versus K_g value

station	liquefaction depths by using Seed & Idriss method (m)	K_g value	station	liquefaction depths by using Seed & Idriss method (m)	K_g value
B01	2–4.5 and 5.5–8 and 8.5–10.5	7.51	B28	5.5–8	5.51
B02	5-10	7.01	B30	–	1.25
B04	–	2.53	B32	–	4.74
B05	5.5–7	5.21	B35	3–6 and 6.5–10.5	14.6
B07	–	4.80	B37	6.5–9.5	6.61
B09	–	4.63	B39	–	4.7
B11	–	1.53	B42	5–12	8.14
B12	5–6.5& 8–9.5	6.15	B43	4.5–7 and 8–10	7.19
B15	–	4.63	B44	7–8	5.2
B18	–	1.10	B45	4–6.5	5.17
B19	6–7 and 9–10	5.93	B50	4–6 and 7–8 and 8.5–9.5	6.79
B22	–	3.65	B52	3.5-5 and 6.5-10.5	11.57
B23	8.5–10.5	5.42	B56	6.5–11	8.34
B25	3–4 and 4.5-5 and 5.5–8 and 8.5–10.5	10	B57	–	1.92
B27	–	4.12	B58	–	1.16

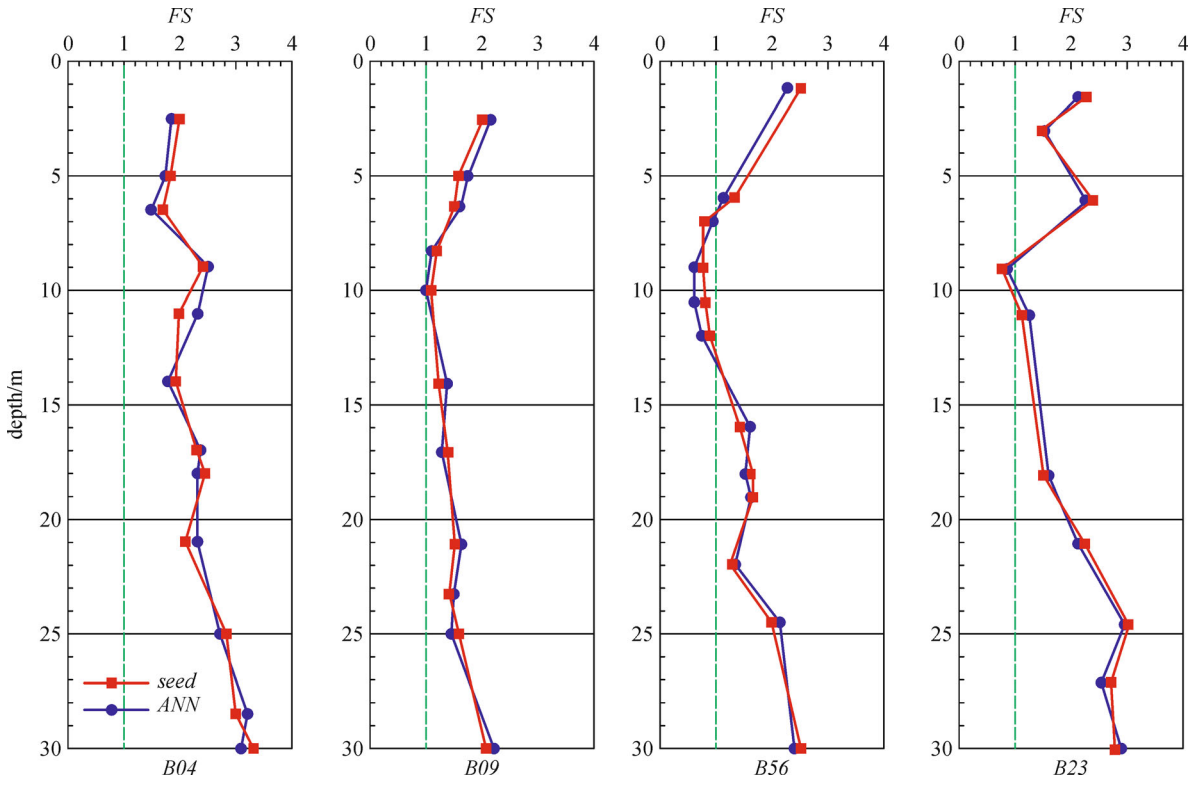

Fig. 9 Evaluation of factor of safety using conventional and ANN method

[40] developed PNN models to analyze the database based on cone penetration test and shear wave velocity data. Ural and Saka [41] developed a BPNN model based on liquefaction records of earthquakes from Japan, China, North and South America. Hsein Juang et al. [42] developed two BPNN models using model-based and actual field results to compare Olsen and Robertson methods for liquefaction potential evaluations. Barai and Agarwal [43] investigated Instance Based Learning, IBL, and models to assess soil liquefaction potential. Hanna et al. [44] explored the efficiency of group piles in cohesionless soil using artificial neural networks. Cha et al. [45] developed ANN to prediction of maximum wave-induced liquefaction in porous seabed.

Considering that ANN can assess liquefaction potential in this precise manner, we will assess the liquefaction phenomena by this method in the 20 remaining stations and the results will be compared with the microtremor measurement result.

6.1 Modeling using MLP-type neural networks

Unknown function approximation has attracted a great deal of research from different areas such as statistic, data mining and engineering sciences. Among various types of function approximation tools, artificial neural networks provide a framework which can learn or approximate any function from a series of given data through a training process [5,36,37]. In addition, the function representation generated by neural networks can be easily used to estimate the relationship between inputs and outputs. Various neural network architectures exist, of which the most popular is the feed-forward multi-layer perceptron (MLP). An MLP type of neural network consists of one input layer; one or more hidden layer(s) and one output layer with a large number of inter connected neurons [46,47]. Figure 10 shows the basic structure of a typical MLP network.

Back-propagation (BP) was originally proposed by Werbos [48] which is based on searching an error surface (error as a function of ANN weights) using the gradient descent algorithm for points with minimum error. In this investigation Back-propagation method is applied to train the ANN which is the most widely used learning process in neural networks today.

6.2 Performance of ANN

The most common parameters for evaluation of a neural network's performance are root mean squared error (RMSE) and mean absolute error (MAE) [40]. MAE and RMSE errors are defined as

$$\text{RMSE error}: \sqrt{\frac{\sum_{i=1}^{n}(Des_i - Est_i)^2}{n}}, \tag{11}$$

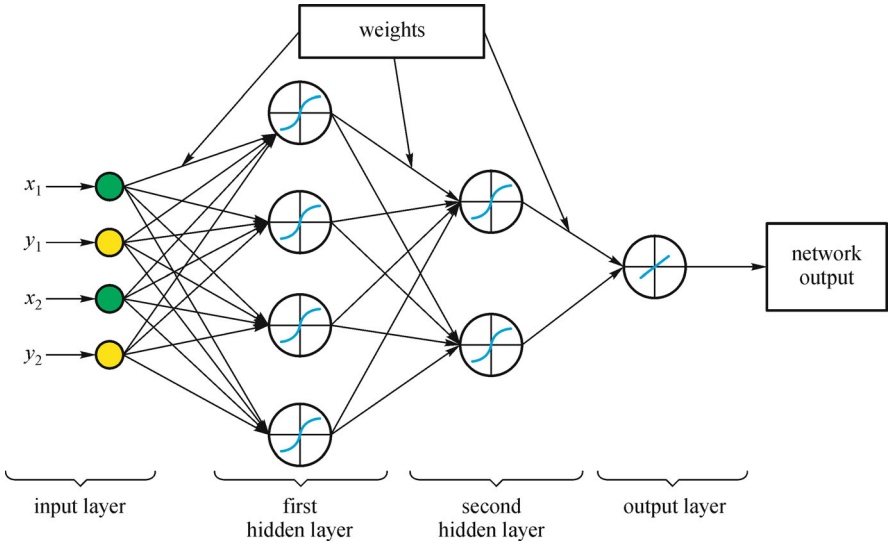

Fig. 10 The structure of a MLP-type network

$$\text{MAE error}: \frac{\sum_{i=1}^{n} |Des_i - Est_i|}{n}, \tag{12}$$

where n is the number of training data, Des_i is desired output and Est_i is estimated output. The number of hidden layers and the neurons in each of them should be determined in a way to minimum the above errors.

6.3 Assessment and comparison of liquefaction potential by using ANN

The input–output data pairs used in the present work consist of four input variables, including soil type, total stress, effective stress, corrected SPT blow count and one output factor of safety. Before using the training procedure the data were normalized to their mean value and standard deviation 1. A training set of 23 out of 30 input–output data pairs is used to train the MLP-type neural network with only one hidden layer based on BP algorithm [5,46,47]. In addition to 30 inputs utilized for training and testing purposes, 6 inputs were also used for validation control in order to prevent over learning. There are many activation functions in the refrences [5,46,47]. The tests showed that the tangent hyperbolic function between input layer and hidden layer have the best function. Also, the linear activation function between hidden layer and output layer has the best function.

At the end of the training process, it is necessary to evaluate the capability of ANN model in prediction of liquefaction potential. The remaining 7 data pairs are used to test the network performance. Since there are four input variables the network has four neurons in the input layer and one neuron in the output layer. Hence there is no specific method to determine the number of neurons in the hidden layer, Trial and error was used. Considering the refrences suggestions [5,46,47] one method for determining the number of neurons in the hidden layer is the gradual increase of the number of neurons and reviewing the amount of ANN's error. In the present research, the aim method has been used. As it is observed in the Fig. 11, the 15 neurons have the least network error and by increasing or decreasing the number of neurons in the ANN, the rate of error increase.

Figure 12 depicts the effect of different neural network architecture (different number of neurons in the hidden layer) on the RMS error of the network obtained from the normalized data. As can be seen a network with 15 neurons in the hidden layer has an acceptable performance.

The excellent behavior of the MLP-type neural network is shown in Fig. 9. Also, Fig. 13 shows regression value obtained between result of ANN and available data. So, the trained network can model and predict the outputs successfully. It is evident from test data sets that the experimental ANN can be applied successfully to predict liquefaction potential.

Figure 14 shows regression value obtained between result of ANN that trained with normalized data and available data. The regression value is 0.978 and 0.937 for the normalized inputs and the non-normalized inputs, respectively, which shows that the trained ANN has a better function with the normalized inputs.

The excellent behavior of the MLP-type neural network for both training and testing data for the present case is also shown in Fig. 15. The figure reveals that the trained network is able to model and predict the outputs successfully.

Table 3 Data sets with inputs and output values with indicating the training and testing sets

borehole number	soil type	total stress	effective stress	N-SPT	FS
1	CL	195	152	25	1.9
2	CH	175	134	23	1.8
3	SM	133	118	7	0.7
4	CH	145	108	16	1.5
5	CL	201	163	26	1.9
6	SC	144	111	13	1.3
7	SC	165	155	5	0.55
8	CL	222	174	29	2.2
9	CH	217	178	26	2.1
10	CL	158	123	12	1.1
11	CL	195	158	27	1.9
12	GW	176	144	14	1.1
13	CL	235	190	30	2.3
14	SM	195	151	25	1.9
15	CH	243	200	24	2
16	SC	139	123	8	0.85
17	CL	185	143	22	1.7
18	CH	197	155	24	1.9
19	CH	189	145	23	2
20	CL	165	129	26	1.8
21	SM	145	131	9	0.9
22	CH	156	119	18	1.25
23	SC	139	121	8	0.8
24	SM	161	127	22	1.5
25	GW	142	120	8	0.9
26	SM	195	161	15	1.3
27	CH	226	188	30	2.1
28	SC	143	138	5	0.6
29	SC	131	119	6	0.8
30	SM	152	117	16	1.3

Table 4 Inputs and output ranges for training data sets used for construction of ANN model

range	input			output	
	soil type	total stress	effective stress	*N-SPT*	*FS*
max	-	243	200	30	2.30
min	-	133	108	5	0.55
ave	-	179	145	19	1.58

Table 5 Inputs and output ranges for testing data sets used for construction of ANN model

range	input			output	
	soil type	total stress	effective stress	*N-SPT*	*FS*
max	-	226	188	30	2.1
min	-	131	117	5	0.6
ave	-	164	139	15	1.21

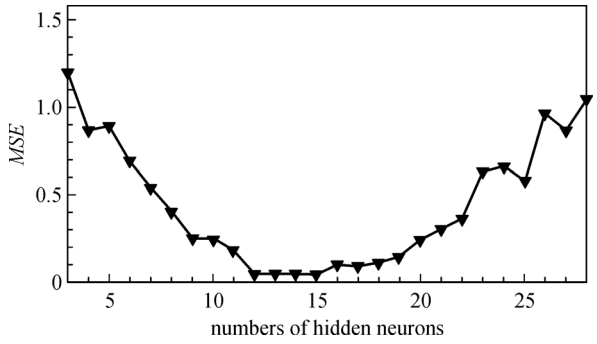

Fig. 11 Maximum squared error versus number of hidden layer neurons

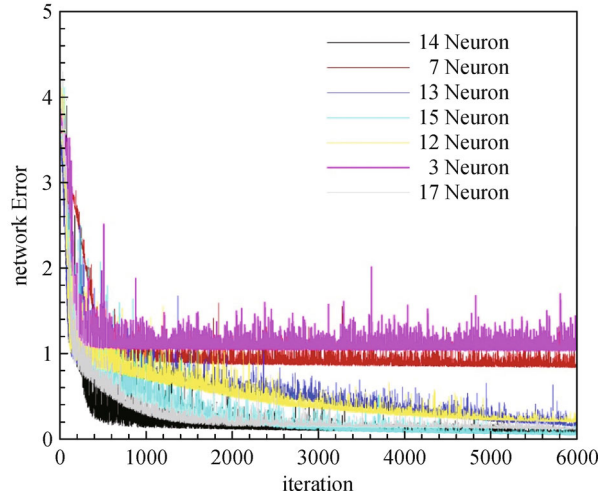

Fig. 12 Effects of the number of hidden neurons on the network performance

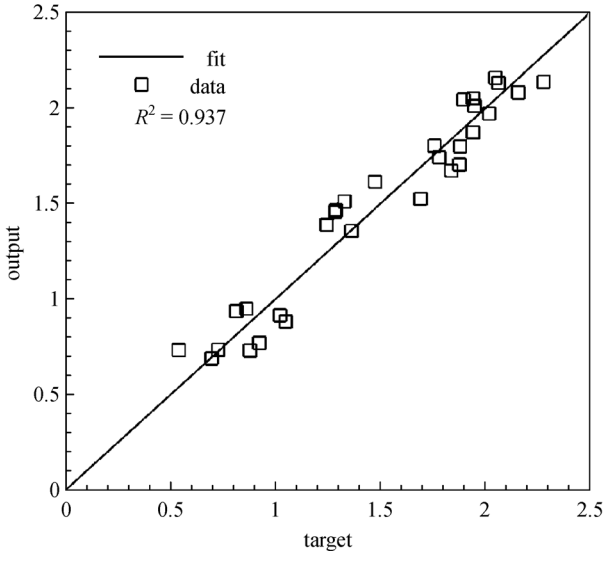

Fig. 13 Performance of ANN in term of regression value

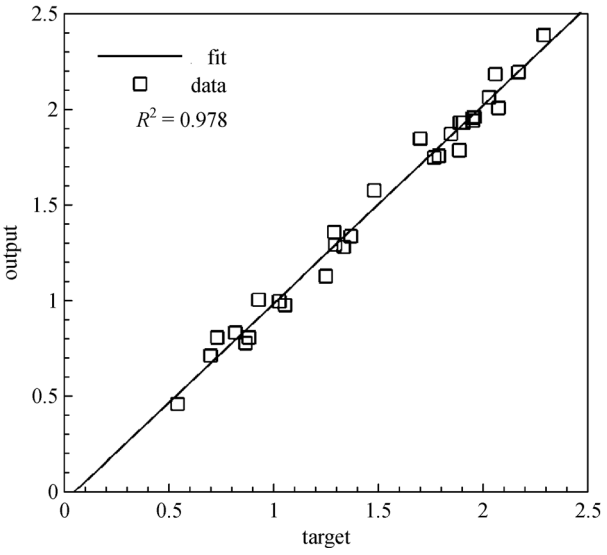

Fig. 14 Performance of ANN in term of regression value (normalized value of data)

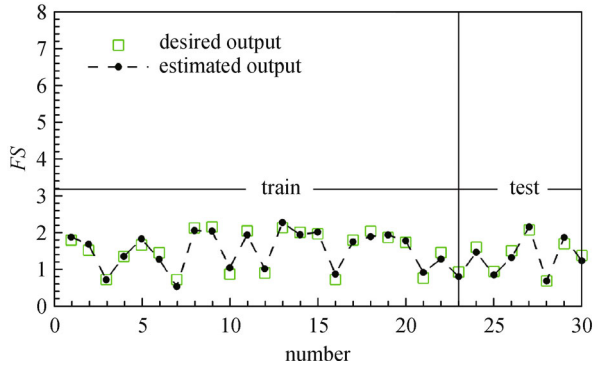

Fig. 15 ANN prediction for the *FS* for all boreholes

Figure 16 compare error values for controlling competency of the ANN models in training and testing data sets. The regression value is 0.939 and 0.943 for the test and train, respectively.

Table 3 shows data sets with inputs and output values with indicating the training and testing sets. Tables 4 and 5 shows the inputs and output ranges for training and testing data sets used for construction of ANN model.

Figure 17 shows the liquefaction microzonation by using microtremor measurements and Fig. 18 indicates the liquefaction microzonation by the ANN. In these two figures, the areas shown in red include the zones with liquefaction potential. By comparing the two methods, it is concluded that they have very good conformity with each other. Only in 4 stations of B32, B36, B44 and B45, the results are different. The K_g value in these stations is close to 5 which is considered the threshold value for liquefaction phenomena. The value of K_g at these stations changes with a minor change in the fundamental frequency

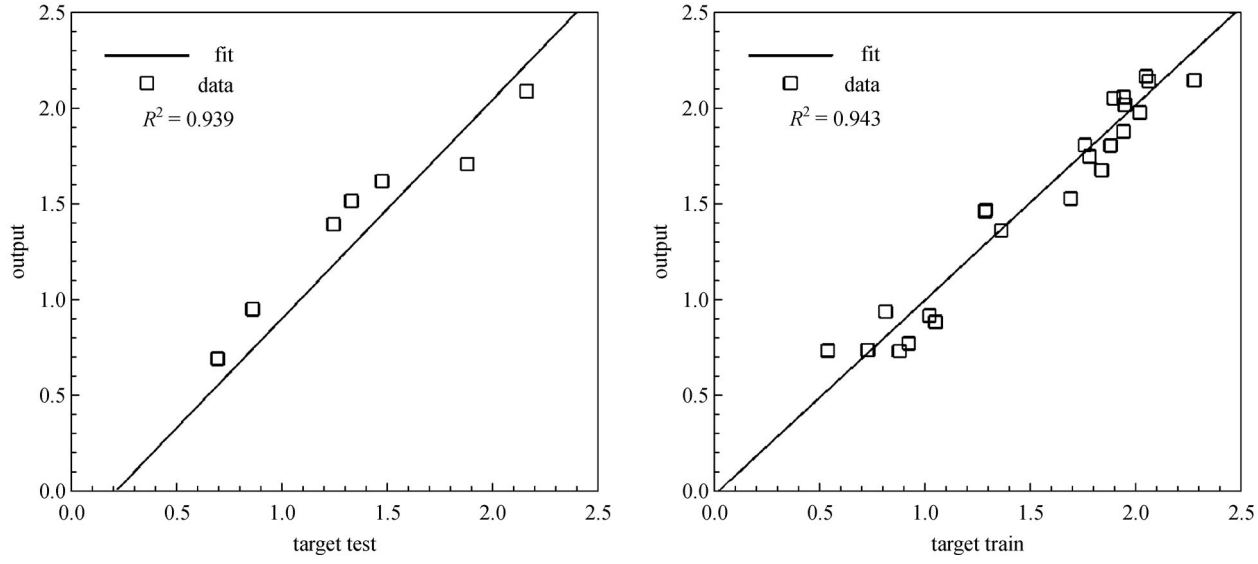

Fig. 16 Regression value for train and test

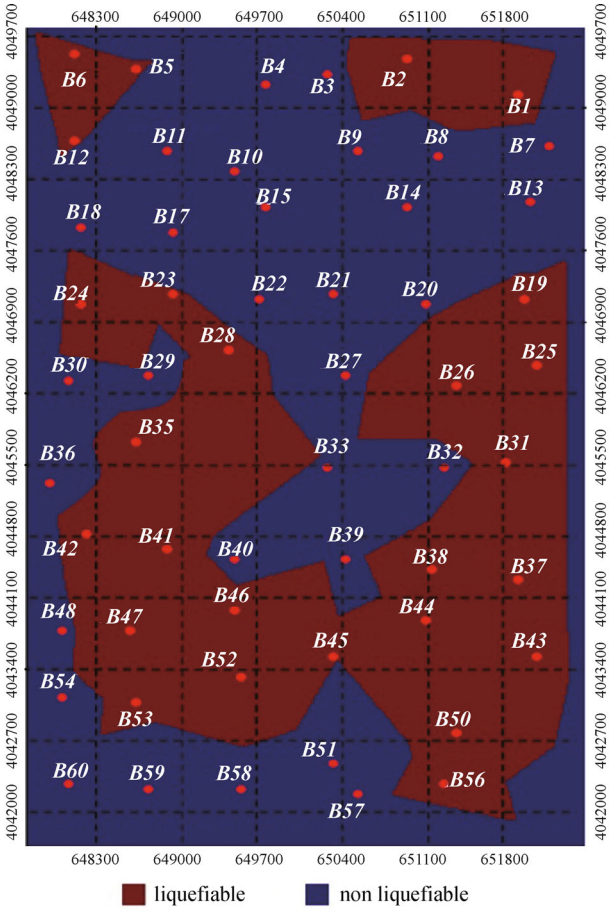

Fig. 17 Liquefaction microzonation of Babol by microtremor

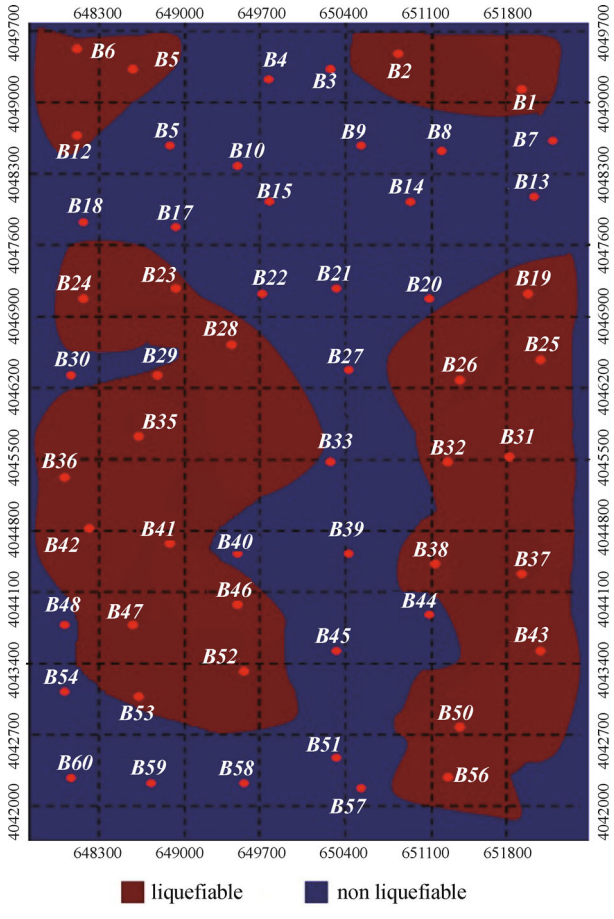

Fig. 18 Liquefaction microzonation of Babol by ANN

and amplification factor. Also, we used the ANN for comparing the two methods which have a small error in prediction. For this reason, the mentioned minor difference is not taken into consideration and the value of $K_g = 5$ is introduced as a threshold value, such that soils with higher K_g values will have liquefaction potential.

From these results, it is reasonable to conclude that K_g is clearly a value which corresponds to the site and can be considered as vulnerability index of that site, an indicator which might be useful in selecting weak points of ground especially in liquefied areas.

7 Conclusion

In the present research, the microtremor measurements were used in 60 stations in order to evaluate the liquefaction potential. By using the fundamental frequency and amplification factor, the value of vulnerability index (K_g) was calculated. To obtain a precise value for K_g which is the threshold value such that at higher values, the liquefaction potential exists, the microtremor results have been compared with the conventional method results. By comparing these results, it is concluded that in Babol city, the stations with K_g values higher than 5, have the liquefaction potential. Subsequently, in order to assess the liquefaction potential, the ANN was utilized in the remaining stations. By comparing the ANN and microtremor results, it was observed that the results are in good conformity with each other and except for 4 stations, the liquefaction phenomena has occurred in all those other stations where their K_g values were higher than 5. With regards the results of the three methods, we can conclude the threshold value of liquefaction potential is $K_g = 5$. Furtheremore, we prepared two maps for liquefaction microzonation by using the microtremor and ANN results. Finally, it can be stated that microtremor measurements are considered suitable and complementary method among conventional methods for reviewing the liquefaction potential which is fast, applicable and cost-effective.

References

1. Seed H B, Idriss I M. Simplified procedure for evaluating soil liquefaction potential. Journal of the Soil Mechanics and Foundations Division, 1971, SM9: 1249–1273
2. Choobbasti A J, Rezaei S, Farrokhzad F. Evaluation of site response characteristics using microtremors. Gradevinar, 2013, 65: 731–741
3. Choobbasti A J. Numerical simulation of liquefaction. Dissertation for the Doctoral Degree. Manchester: University of UMIST, 1997
4. Nakamura Y. A method for dynamic characteristics estimation of subsurface using microtremor on the ground surface. Quarterly Report of RTRI, 1989, 30: 25–33
5. Rezaei S, Choobbasti AJ, Soleimani Kutanaei S. Site effect assessment using microtremor measurement, equivalent linear method and artificial neural network (Case study: Babol, Iran), Arab J of Geosci, 2013 (DOI: 10.1007/s12517-013-1201-1)
6. Paudyal Y R, Yatabe R, Bhandary N P, Dahal R K. Basement topography of the Kathmandu Basin using microtremor observation. Journal of Asian Earth Sciences, 2013, 62: 627–637
7. Fnais M S, Abdelrahman K, Al-Amri A M. Microtremor measurements in Yanbu city of Western Saudi Arabia: A tool for seismic microzonation. J King Saud Univ, 2010, 22(2): 97–110
8. Beroya MAA, Aydin A, Tiglao R, Lasala M. Use of microtremor in liquefaction hazard mapping. Eng Geo, 2009, 107: 140–153
9. Saygili G. Liquefaction potential assessment in soil deposits using artificial neural network. Master Thesis, Montreal: Concordia University, 2005
10. Nakamura Y. Real-time information systems for hazard mitigation. In: Proceedings of the 10th World Conference in Earthquake Engineering. Spain, Madrid, 1996
11. Huang H C, Tseng Y S. Characteristics of soil liquefaction using H/V of microtremors in Yuan-Lin area, Taiwan. TAO, 2002, 13(3): 325–338
12. Farrokhzad F, Choobbasti A J, Barari A. Liquefaction microzonation of Babol city using artificial neural network. J King Saud Univ Sci, 2012, 24(1): 89–100
13. Choobbasti AJ, Rezaei S, Farrokhzad F, Azar P. Evaluation of site response characteristics using nonlinear method (Case study: Babol, Iran), Front Struct Civ Eng. 2014, 8(1): 69–82
14. Kanai K, Takana T. On microtremors. VIII. Bull Earth Research Int, 1961, 39: 97–114
15. Dikmen U, Mizaoglu M. The sesimic microzonation map of Yenisehir-Bursa, NW of Turket by means of ambient noise measurements. J Balkan Geoph Soc, 2005, 8: 53–62
16. Rezaei S. Assessing the site effects and estimation of strong ground motion specification by using microtremor data and compare its results with simulation of soil profile (Case study: western part of Babol city). Master Thesis, Babol: Babol Noshiravani University of Technology, 2014
17. Toshinawa T, Inoue M, Yoneyama N, Hoshino Y, Mimura K, Yokoi Y. Geologic-profile estimates of Kofu Basin, Japan, by making use of microtremor observations. Geophysical Research Abstracts, 2003, 5: 02079
18. Maruyama Y, Yamazaki F, Hamada T. Microtremor measurements for the estimation of seismic motion along expressway. In: Proceedings of the 6th International Conference of Seismic Zonation. Palm Springs, USA, California, 2000
19. Nakamura Y. Clear identification of fundamental idea of Nakamura's technique and its applications. In: Proceedings of the 12th World Conference on Earthquake Engineering. Auckland, New Zealand, 2000
20. Bour M, Fouissac D, Dominique P, Martin C. On the use of microtremor rcordings in seismic microzonation. Soil Dynamics and Earthquake Engineering, 1998, 17(7–8): 465–474
21. Teves-Costa P, Matias L, Bard P Y. Seismic behavior estimation of thin alluvium layers using microtremor recordings. Soil Dynamics and Earthquake Engineering, 1996, 15(3): 201–209
22. Field E H, Hough S H, Jacob K. Using microtremors to assess potential 16-earthquake site response: A case study in Flushing

Meadows, New York City. Bulletin of the Seismological Society of America, 1990, 80: 1456–1480
23. Harutoonian P, Leo C J, Doanh T, Castellaro S, Zou J J, Liyanapathirana D S, Wong H, Tokeshi K. Microtremor measurements of rolling compacted ground. Soil Dynamics and Earthquake Engineering, 2012, 41: 23–31
24. Gosar A. Microtremor HVSR study for assessing site effects in the Bovec basin (NW Slovenia) related to 1998 M_w5.6 and 2004 M_w5.2 earthquakes. Engineering Geology, 2007, 91(2–4): 178–193
25. Zhao B, Xie X, Chai C, Ma H, Xu X, Peng D, Yin W, Tao J. Imaging the garben structure in the deep basin with a microtremor profile crossing the Yinchuan City. Journal of Geophysics and Engineering, 2007, 4(3): 293–300
26. Chávez-García F J, Kang T S. Lateral heterogeneities and microtremors: Limitations of HVSR and SPAC based studies for site response. 2014, 174: 1–10
27. Deif A, El-Hadidy S, Sayed S R M, El Werr A. Definition soil characteristics and ground response at the northewerstern part of Gulf of Suez, Egypt. Journal of Geophysics and Engineering, 2008, 5(4): 420–437
28. Nakamura Y. Seismic vulnerability indices for ground and structures using Microtremor. World Congress on Railway Research, Italy, Florence, 1997
29. Uehan F, Nakamura Y. Ground motion characteristics around Kobe City detected by microtremor measurement. In: Proceedings of the 11th World Conference on Earthquake Engineering. Acapulco. Mexico, 1996
30. Saita J, Nakamura Y, Sato T. Liquefaction caused by the 2011 off the Pacific coast of Tohoku earthquake and the result of the prior microtremor measurement. In: Proceedings of the 9th International Conference on urban earthquake engineering. Tokyo, Japan, 2012
31. Walling M Y, Mohanty W K, Nath S K, Mitra S, John A. Microtremor survey in Talchir, India to ascertain its basin characteristics in terms of predominant frequency by Nakmaura's ratio technique. Engineering Geology, 2009, 106(3–4): 123–132
32. Bolton Seed H, Tokimatsu K, Harder L F, Chung R M. Influence of SPT procedures in soil liquefaction resistance evaluations. Journal of Geotechnical Engineering, 1985, 111(12): 1425–1445
33. Jha S K, Suzuki K. Reliability analysis of soil liquefaction based on standard penetration test. Computers and Geotechnics, 2009, 36(4): 589–596
34. Youd T L, Idriss I M, Andrus R D, Arango I, Castro G, Christian J T, Dobry R, Finn W D L, Harder L F Jr, Hynes M E, Ishihara K, Koester J P, Liao S S C, Marcuson W F III, Martin G R, Mitchell J K, Moriwaki Y, Power M S, Robertson P K, Seed R B, Stokoe K H II. Liquefaction resistance of soils; summary report from the 1996 NCEER and 1998 NCEER/NSF workshops on evaluation of liquefaction resistance of soils. Journal of Geotechnical and Geoenvironmental Engineering, 2001, 127(10): 817–833
35. Choobbasti A J, Farrokhzad F, Barari A. Predicting Subsurface Soil Layering and Landslide risk with Artifical Neural Network a Case Study from Iran. Geologica Carpath, 2011, 5: 1–16
36. Vu-Bac N, Lahmer T, Keitel H, Zhao J, Zhuang X, Rabczuk T. Stochastic predictions of bulk properties of amorphous polyethylene based on molecular dynamics simulations. Mechanics of Materials, 2014, 68: 70–84
37. Vu-Bac N, Lahmer T, Zhang Y, Zhuang X, Rabczuk T. Stochastic predictions of interfacial characteristic of carbon nanotube polyethylene composites. Composites. Part B, Engineering, 2014, 59: 80–95
38. Goh A T C. Empirical design in geotechnics using neural networks. Geotechnique, 1995, 45(4): 709–714
39. Goh A T C. Neural network modeling of CPT seismic liquefaction data. J Geotech Geoenviron Eng Div, 1996, 122(1): 70–73.
40. Goh A T C. Probabilistic neural network for evaluating seismic liquefaction potential. Canadian Geotechnical Journal, 2002, 39(1): 219–232
41. Ural D N, Saka H. Liquefaction assessment by neural networks. Elect J Geotech Eng, 1989 (http://geotech.civen.okstate.edu/ejge/ppr9803/index.html)
42. Hsein Juang C, Chen C J, Tien Y M. Appraising cone penetration test based liquefaction resistance evaluation methods: Artificial neural network approach. Canadian Geotechnical Journal, 1999, 36 (3): 443–454
43. Barai S, Agarwal G. Studies on isnstance based learning models for liquefaction potential assessment, Elect J Geotech Eng, 2002 (http://www.ejge.com/2002/Ppr0235/Ppr0235.htm)
44. Hanna A M, Morcous G, Helmy M. Efficiency of pile groups installed in cohesionless soil using artificial neural networks. Canadian Geotechnical Journal, 2004, 41(6): 1241–1249
45. Cha D, Zhang H, Blumenstein M. Prediction of maximum wave-induced liquefaction in porous seabed using multi-artificial neural network model. Ocean Engineering, 2011, 38: 878–887
46. Tavakoli H, Omran O L, Kutanaei S S, Shiade M S. Prediction of energy absorption capability in fiber reinforced self-compacting concrete containing nano-silica particles using artificial neural network. Latin American Journal of Solids and Structures, 2014, 11 (6): 966–979
47. Choobbasti A J, Tavakoli H, Kutanaei S S. Modeling and optimization of a trench layer location around a pipeline using artificial neural networks and particle swarm optimization algorithm. Tunnelling and Underground Space Technology, 2014, 40: 192–202
48. Werbos P J. Beyond regression: New Tools for Prediction and Analysis in the Behavioural Sciences, Dissertation for the Doctoral Degree. Canbridge: Harvard University, 1974